scientific reports

Check for updates

OPEN

Microfluidics chips fabrication techniques comparison

Xiaocheng Liu[1], Antao Sun[1], Jan Brodský[2], Imrich Gablech[2]✉, Tomáš Lednický[2], Petra Vopařilová[3], Ondřej Zítka[3], Wen Zeng[1]✉ & Pavel Neužil[1]✉

This study investigates various microfluidic chip fabrication techniques, highlighting their applicability and limitations in the context of urgent diagnostic needs showcased by the COVID-19 pandemic. Through a detailed examination of methods such as computer numerical control milling of a polymethyl methacrylate, soft lithography for polydimethylsiloxane-based devices, xurography for glass-glass chips, and micromachining-based silicon-glass chips, we analyze each technique's strengths and trade-offs. Hence, we discuss the fabrication complexity and chip thermal properties, such as heating and cooling rates, which are essential features of chip utilization for a polymerase chain reaction. Our comparative analysis reveals critical insights into material challenges, design flexibility, and cost-efficiency, aiming to guide the development of robust and reliable microfluidic devices for healthcare and research. This work underscores the importance of selecting appropriate fabrication methods to optimize device functionality, durability, and production efficiency.

The field of microfluidics has seen remarkable advancements in the last few decades and has become an irreplaceable part of complex tools in healthcare, environmental monitoring, and chemical engineering[1]. The microfluidic chip is the core of this transformative technology, a miniaturized system capable of precisely handling small fluid volumes[2]. The design and performance of these chips[3] are critically influenced by the fabrication techniques employed, each with its unique set of advantages and limitations. Alongside some of the more common fabrication techniques, several alternative methods have been explored, such as hot embossing, 3D printing, laser ablation, and paper-based microfluidics[4]. Hot embossing, for example, is particularly useful for thermoplastic materials, offering high throughput but requiring initial mold fabrication[5]. 3D printing is an additive manufacturing technique that allows for high design flexibility but often suffers from resolution limitations and is time-consuming[6]. Laser ablation can generate microchannels with high precision but is also time-consuming and can produce undesirable thermal effects that might alter material properties[7].

Nevertheless, the laser ablation technique is widely used for mass-produced microfluidics chips for electrochemical blood sugar monitoring[8] and detecting biomarkers such as prothrombin for implant rejection/acceptance[9]. Paper-based microfluidics[10] offer an incredibly cost-effective approach and portability, typically limited to more straightforward assays and fluidic operations. As the applications of microfluidic devices broaden, there is a growing need to understand the pros and cons of these different technologies used for their fabrication.

Layered stainless steel fabrication involves the stacking and joining metal layers to create complex microchannel networks, benefiting from the material's durability and resistance to harsh conditions. This method is suited for high-pressure or temperature applications and can achieve microscale precision. However, the process can be costly due to the metalworking and involved bonding technologies[11].

Polyimide, a high-performance polymer, is a versatile substrate in microfluidic applications due to its excellent chemical resistance and thermal stability[12]. Techniques such as laser cutting and photolithography are commonly used to shape polyimide into desired microfluidic structures[12]. These methods enable the production of flexible and heat-resistant microfluidic chips, but the fabrication process of the microfluidic chips is rather complex; the surface of the microchannel has a high level of roughness, and the size of the microchannel cannot be precisely controlled[13] in comparison with MEMS machining-based microfluidic chip fabrication.

Silicon-glass devices often rely on anodic bonding techniques, offering excellent chemical resistance and optical transparency. These devices are well suited for applications requiring high-temperature or aggressive

[1]Ministry of Education Key Laboratory of Micro and Nano Systems for Aerospace, School of Mechanical Engineering, Northwestern Polytechnical University, 127 West Youyi Road, Xi'an 710072, Shaanxi, People's Republic of China. [2]Department of Microelectronics, Faculty of Electrical Engineering and Communication, Brno University of Technology, Technická 3058/10, Brno 616 00, Czech Republic. [3]Department of Chemistry and Biochemistry, Mendel University in Brno, Zemědělská 1, Brno 613 00, Czech Republic. ✉email: imrich.gablech@vutbr.cz; zengwen@nwpu.edu.cn; pavel.neuzil@nwpu.edu.cn

chemical reagents. However, they come with a higher production cost and longer fabrication cycles, limiting their suitability for rapid prototyping or low-cost applications[14,15].

Soft lithography, specifically for polydimethylsiloxane (PDMS)-based devices[16], has been a pioneering technology, providing a perfect blend of flexibility, biocompatibility, and rapid prototyping capabilities. PDMS devices are extensively used for biological applications due to their inert nature and low absorption of small molecules[17–19]. Even though they are trendy for microfluidics chip fabrication, they are not very suitable from a material point of view. According to the literature, the PDMS material is soft as its Young's modulus is only a few MPa[20]. While the micro fluids are flowing along the PDMS microchannel, there are some deformations due to the driving pressure force. In addition, the PDMS material also suffers from gas permeability, and difficulties in achieving long-term stable bonding with glass or plastic substrates pose challenges[21–23]. Furthermore, PDMS is incompatible with standard micromachining methods since it is considered a potent vacuum contaminant.

In recent years, paper-based microfluidics has become a rapidly developing research field and microfluidic device fabrication method due to its simplicity, low cost, and portability[24,25]. Paper-based microfluidics has various applications for point-of-care diagnostics, including blood separation and environmental testing[26–28]. However, compared with soft lithography and other techniques, the fabrication precision of the paper-based microfluidic device is not so high. It cannot satisfy the applications requiring microfluidic chips with the precision of chip fabrication.

Xurography, on the other hand[29], offers a cost-effective and rapid fabrication method suitable for educational settings or initial proof-of-concept designs. This technique can generate single-layer microfluidic devices using simple materials like double-sided tapes and commercial cutting plotters. However, xurography is not a precise fabrication technology and often suffers from limitations in achievable feature sizes. Therefore, xurography is unsuitable for applications requiring high fabrication precision or complex 3D microstructures of the microchannel.

Polymethylmethacrylate (PMMA) devices fabricated by injection molding, hot embossing, or computer numerical control (CNC), typically vertical milling, have recently gained attention due to their excellent optical clarity, mechanical stability, and lower costs compared to silicon-based systems[30,31]. Injection molding is advantageous for mass production but comes with high initial mold costs for manufacturing and longer turnaround times for mold fabrication. CNC machining provides more flexibility for rapid prototyping and can produce features with high aspect ratios, but the method may be time-consuming and produce waste material[32]. The PMMA and other plastics such as COC, COP, and PET, can be shaped using hot embossing.

The COVID-19 pandemic has triggered a renewed interest in microfluidic devices for point-of-care diagnostics, where rapid, reliable, and low-cost fabrication methods are highly sought-after. PMMA-based devices, owing to their cost-effectiveness and optical properties, along with PDMS systems for their biocompatibility, have shown promising utility regardless of their relatively low thermal conductivity when used for assays such as polymerase chain reactions (PCR). Heat transfer rate is a critical parameter for assays such as PCR, making their utilization challenging but possible[33]. The Si-glass microfluidics chips, having incorporated Si substrate with its outstanding thermal conductance, have better performance, but their cost is prohibitively high[34,35]. Utilizing low thermal conductivity materials for isothermal nucleic acid amplification, such as loop-mediated isothermal amplification (LAMP) or RPA, has no problem as thermal cycling is eliminated and increased temperature is kept constant[33]. Another option for using plastic for the PCR systems has been demonstrated first by Cepheid[36] and later on by Coyote Bioscience[37] uses injection-molded plastic with extra thin walls of a PCR chamber to improve heat transfer through the plastic. Here, in Table 1 we summarized the materials and methods used for microfluidic chip fabrication.

Material	Method	Minimum feature size	Cost	Durability	Chemical resistance	Ref.
PMMA	CNC Machining	50 µm	Low	Low	Very low	38
	Hot Embossing	50 nm	Very low			5,39
COC	Hot Embossing	50 nm	Low	Low	Low	40
	Injection molding	5 µm	Very low			41
PET	Hot Embossing	50 nm	Low	Moderate	Moderate	39,42
	Injection molding	5 µm	Very low			39
PDMS	Soft lithography	Sub µm	Low	Moderate	High	43
Glass	Wet/dry etching	5–10 µm	High	High	Very high	44
Si-glass	Micromachining and anodic bonding	1 µm	High	High	Very high	45
Stainless steel	Layered fabrication	5–10 µm	Moderate	Very high	Moderate	46
PI	Laser cutting, lithography	10 µm	Low	High	High	47
COP	Injection molding	10 µm	Low	Moderate	Moderate	36,37
PC	Laser machining	50 µm	Very low	Low	Low	8
	3D printing	50 µm	Very low			48
	Hot embossing					39

Table 1. Materials and methods used for microfluidic chip fabrication. COC stands for cyclic olefin copolymer, PET for polyethylene terephthalate, and COP for cyclic olefin polymer.

Understanding the complexity of these fabrication technologies is critical for all microfluidics-based applications and their future improvement and development. In this context, our manuscript aims to clarify the technological problematics associated with the fabrication of microfluidic chips, thereby providing a comparative guide for researchers and engineers in the field. This contribution provides a comparison of various fabrication methods of the microfluidic chips, with a particular focus on CNC machining for PMMA-based microfluidic devices, xurographically fabricated microfluidic systems, soft lithography for PDMS microfluidic chips, and silicon-glass microfluidic devices.

Microfluidic chip fabrication and testing techniques.

Chip design

We designed the chip using a JAVA-based script in a Nanolithography Toolbox software[49], generating a file in graphic design system II (GDSII) format. The design consisted of a few features developed explicitly for microfluidics, such as a chamber with a tangential connection and a rounded path to deliver fluid to a chamber[3] with minimal dead volume. The complete layout script is in the Supplementary online. The main system feature is a polymerase chain reaction (PCR) chamber with a nominal volume of ≈6 µL with an assumption of chamber depth of 100 µm. Besides that, there are also two small chambers, one to capture magnetic particles and a second for magnetic particle purification by oil (Fig. 1).

PDMS chip fabrication

The GDSII file was converted via DXF into a stereolithography file format (STL) using a computer-aided design (CAD) program. Then, we used this file to make a stereolithography 3D printed mold of epoxy that was adopted for fast prototyping. We created a mold for the channel with a width and height of ≈0.4 mm and ≈0.1 mm, respectively. We mixed the PDMS with a two-compound elastomer kit SYLGARD® 184 (Dow Chemical, USA) with a standard mixing weight ratio of 10:1. Subsequently, the prepared mixture was degassed in a vacuum desiccator and cast in a thickness of ≈4 mm over the mold. The first curing was performed at room temperature to avoid the deformation of the epoxy mold for ≈20 h. Then, the cast material was peeled off, cut to a size of (55×25) mm[22], and post-baked at ≈80 °C for two hours to ensure complete cross-linking of the material. A puncher made the port holes with a diameter of ≈1 mm. The surface of these PDMS pieces and ≈1 mm-thick microscopic slides were activated in O_2 plasma for ≈1 min using pressure, plasma radio frequency power, and O_2 flow rates of ≈500 Pa, ≈ 300 W, and ≈20 sccm, respectively. Then, both parts were pressed together to be bonded. As the last step, the fabricated chips were baked for ≈5 min at a hotplate with a temperature of ≈100 °C to increase the bonding strength (Fig. 2).

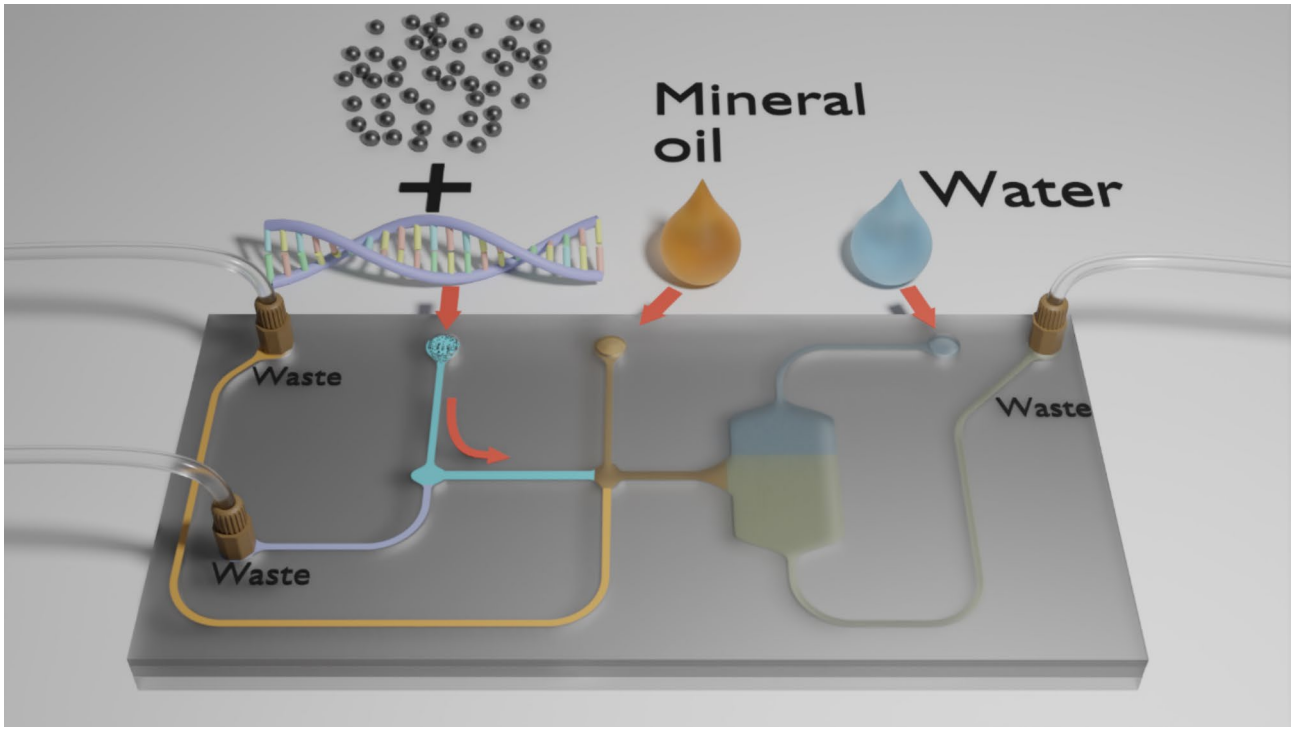

Fig. 1. Schematic representation of the microfluidic chip design featuring a PCR chamber, magnetic particle capture chamber, and purification chamber generated using Nanolithography Toolbox software. The design emphasizes a chamber with tangential connections to minimize dead volume, as detailed in the JAVA-based script in the Supplementary online.

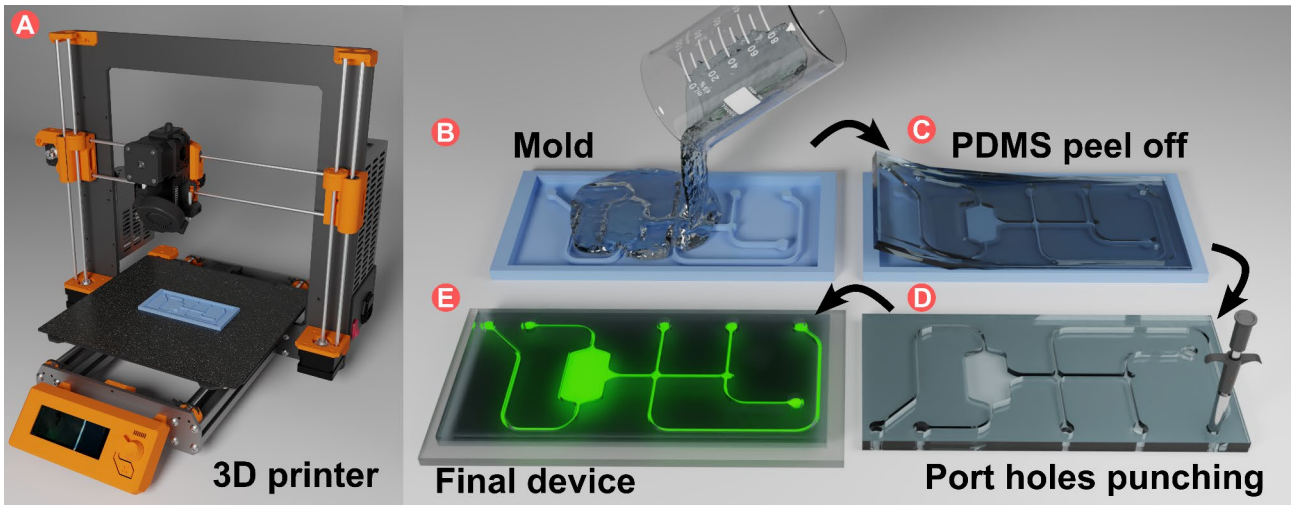

Fig. 2. The process flow for fabricating PDMS microfluidic chips: (**A**) Mold creation using a 3D print. (**B**) PDMS was poured on the mold and its cross-linking. (**C**) Peeling off the PDMS layer. (**D**) Puncturing of fluid access holes. (**E**) Bonding of the PDMS to the glass substrate and filling with fluorescein to increase contrast.

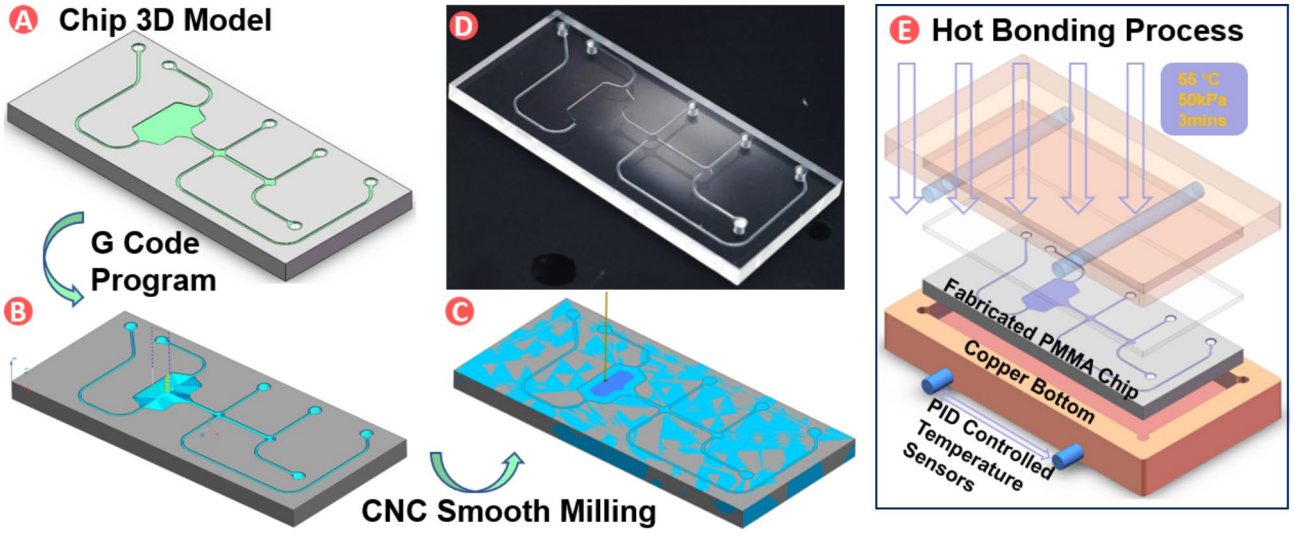

Fig. 3. Overview of the PMMA Microfluidic Chip Fabrication Process - From CNC Milling to Final Assembly: (**A**) The 3D model of the PMMA chip structure formed by converting the DXF file created by the Nanolithography toolbox. (**B**) Computer numerical control (CNC) machine tool path code programming is used to mill PMMA slabs precisely into microfluidic chip layouts. (**C**) Simulation of chip manufacturing process controlled by G code. (**D**) PMMA chip showcasing with microchannels and chambers before bonding is milled using a polish CNC process. (**E**) Aligned flat PMMA slab with channels and the cover slab for bonding by a custom-built pneumatic thermal press for low-temperature, chemically assisted PMMA components.

PMMA chip fabrications

We made microfluidic chips made by conventional CNC milling from PMMA. We first converted the GDSII files into a data exchange format (DXF). We used CAD software to convert 2D DXF into a 3D format called standard for exchanging product data (STEP), a standard file format for CNC machining. The STEP file was converted into a computer-aided machine program, Mach 3, used for vertical milling. We made the chip from ≈3 mm PMMA slabs with a total width and length dimension of (55×25) mm[22]. This chip was bonded to a flat piece of PMMA with a thickness of ≈1 mm by various techniques, such as laser bonding and primarily by chemically assisted thermal bonding[50], a method used in this work.

We combined a previously published chemically assisted low-temperature bonding technique at ≈55 °C with a temperature-controlled pneumatic press[51]. We adopted the originally developed heat stitching and hot embossing system (Fig. 3). As a result, we could perform PMMA boding at low temperatures in ≈3 min.

First, we immersed the CNC-produced chip and the ≈1 mm thick PMMA cover in ethanol for ≈3 min. Then, we aligned their edges to each other, forming a sandwich and placing it on a heated system developed initially for hot embossing. We set the temperature of the press's top and bottom metal plates to ≈55 °C and put the sandwich on the bottom plate, separated from it by ≈2 mm thick silicone rubber. The same rubber was placed on the top of the sandwich, and the press was activated to create a force controlled by an air pressure cylinder with a pressure set to ≈50 kPa while heating the PMMA sandwich to ≈55 °C for ≈3 min (Fig. 3).

Xurographically made microfluidics

As an alternative technique, we used a xurographically patterned double-sided tape. The pattern size of (55×25) mm[22] has also been generated using the Nanolithography toolbox[3] (Fig. 4A) showing part of the script in Fig. 4B and complete layout in Fig. 4C. The microfluidic design is shown in Fig. 4D and the knife-cutting path in Fig. 4E.

The chip was again designed with a reaction chamber suitable for either PCR or loop-mediated isothermal amplification (LAMP), a sample collection chamber, an oil chamber, injection holes, and waste liquid ports. Here, we had to change the pattern resolution to keep a minimal resolution of ≈100 µm due to the limitation of the controlled knife motion (Fig. 4F) during xurography. Then, we converted the pattern from GDSII into DXF format and transferred it to the xurography tool. We cut the double-sided tape with a thickness of ≈200 µm and used it to bond two glasses, one flat with no pattern and one with six drilled holes for fluid access to the microfluidic system together, forming the microfluidic chip. The tape made by Tesa company model Tesa® 61395 is made of a black polyethylene terephthalate (PET) backing and a pressure-sensitive (called tackifier) acrylic adhesive. The initial adhesion to glass is ≈14.3 $N{\cdot}cm^{-1}$; after 14 days, it is increased to ≈16.6 $N{\cdot}cm^{-1}$.[40] We peeled off the area we did not want, and the top layer of the pattern was used to expose the black adhesive layer. Then, we put the glass onto it and squeezed it slightly to attach it to the tape. The glass with holes was then attached to the first glass one with the tape between and gaps in the tape from the microfluidic channels and chambers (Fig. 4G). The process of attaching layers is shown in (Fig. 4H) and complete fabricated microfluidic chip filled with fluorescin solution to enhance the channel contrast in (Fig. 4I).

Silicon-glass microfluidic chips.

We employed a double deep reaction ion etching (DRIE) technique many times before[52]. The Si wafers were first oxidized to grow a thermal SiO_2 layer with the thickness required to serve as a hard mask for DRIE's microfluidic channel etching, utilizing the etching process's selectivity. Then, the first lithography with a photoresist (PR) has a thickness between ≈1 µm and ≈2 µm. Once the PR is developed, the underneath layer's SiO_2 layer is etched either by a buffered oxide etch solution (BOE) or reaction ion etching (RIE). In any case, the etching was stopped at the Si substrate. Then, the second lithography with PR having a thickness of ≈15 µm or more, for the most common wafer thickness of ≈525 µm, is performed to define access holes for the microfluidic system. Subsequently, the Si substrate was etched through the DRIE process, the PR was removed, and the Si wafer was etched again into the desired depth using SiO_2, which was etched before as a mask. BOE entirely removed the SiO_2, the wafer was cleaned, and ≈5 nm of the SiO_2 layer was thermally grown in a furnace to ensure the microfluidic system's well-defined surface. Such a processed wafer was anodically bonded to a Pyrex-

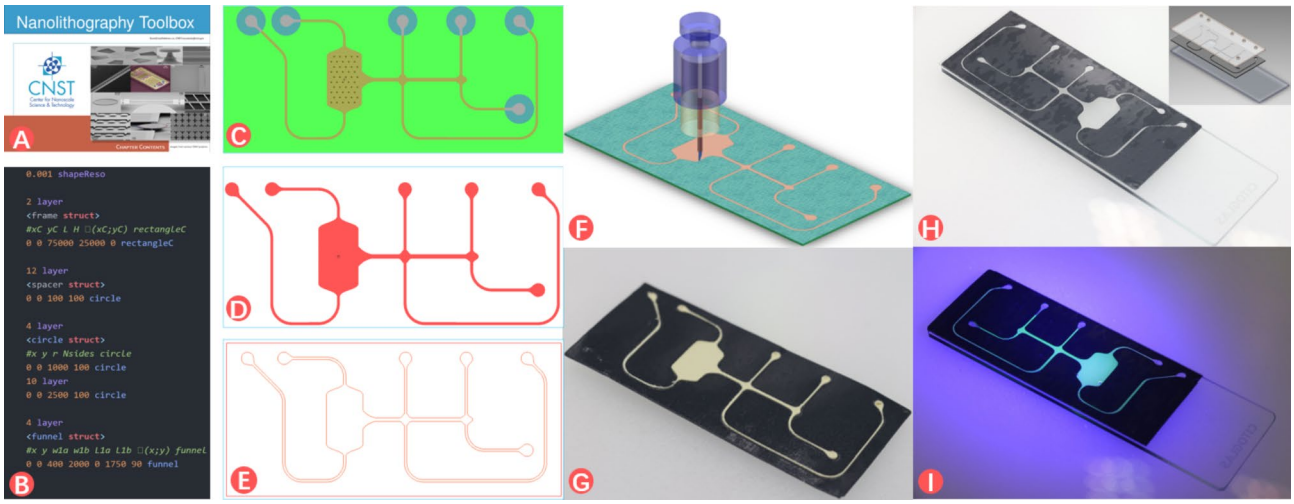

Fig. 4. Fabrication of a Microfluidic Chip via Xurography: (**A**) The Nanolithography toolbox software. (**B**) The code for the generation layer in the gds II formats of chips with microchannels and its cover. (**C**-**E**) The gds II layout is generated by the Nanolithography toolbox code, the main chip layer within the functional microchannel, and the DXF file converted by the GDS layer file. (**F**) This image illustrates the xurography-based fabrication process. The upper cutter displays the xurography tool for cutting the adhesive pattern alongside the pre-cut cover and substrate. (**H**) All layers are aligned and bonded to create the microfluidic channels, as depicted in the assembled chip. (**I**)The last image schematically shows the finished microfluidic device filled with fluorescein dye, demonstrating the successful creation of functional channels under blue light.

type glass, and then the wafer sandwich was diced using a diamond blade dicing saw into individual chips. The entire fabrication process is shown in Fig. 5.

The device fluorescence contrast can be improved by using a relatively expensive silicon-on-insulator substrate, where the depth of the microfluidics channels and chambers is defined by the thickness of the top Si layer[45] and not by time, as it is done with conventional Si substrates. The results are superior to those of the traditional Si substrate-based device, but unfortunately, the cost of SOI substrate makes this technology prohibitive for large and especially disposable chips.

Heat transfer rate

Due to various properties, the heat flux $\Delta Q/\Delta t$ during heating and cooling of the microfluidic chip is governed by an equation:

$$\frac{\Delta Q}{\Delta t} = -k \cdot A \cdot \frac{\Delta T}{\Delta x}, \tag{1}$$

where ΔQ is heat change, Δt is a time change, k is thermal conductance, A is an area, ΔT is temperature difference, and Δx is distance, and the total heat flux heavily depends on the chip material and its thickness. We used fluorescein solution instead of a precise DNA solution with intercalating dye[53] as temperature sensing material and perform heating and cooling of each chip to determine the heat transfer[52,54]. The devices were made of various materials having different thermal properties (Table 2).

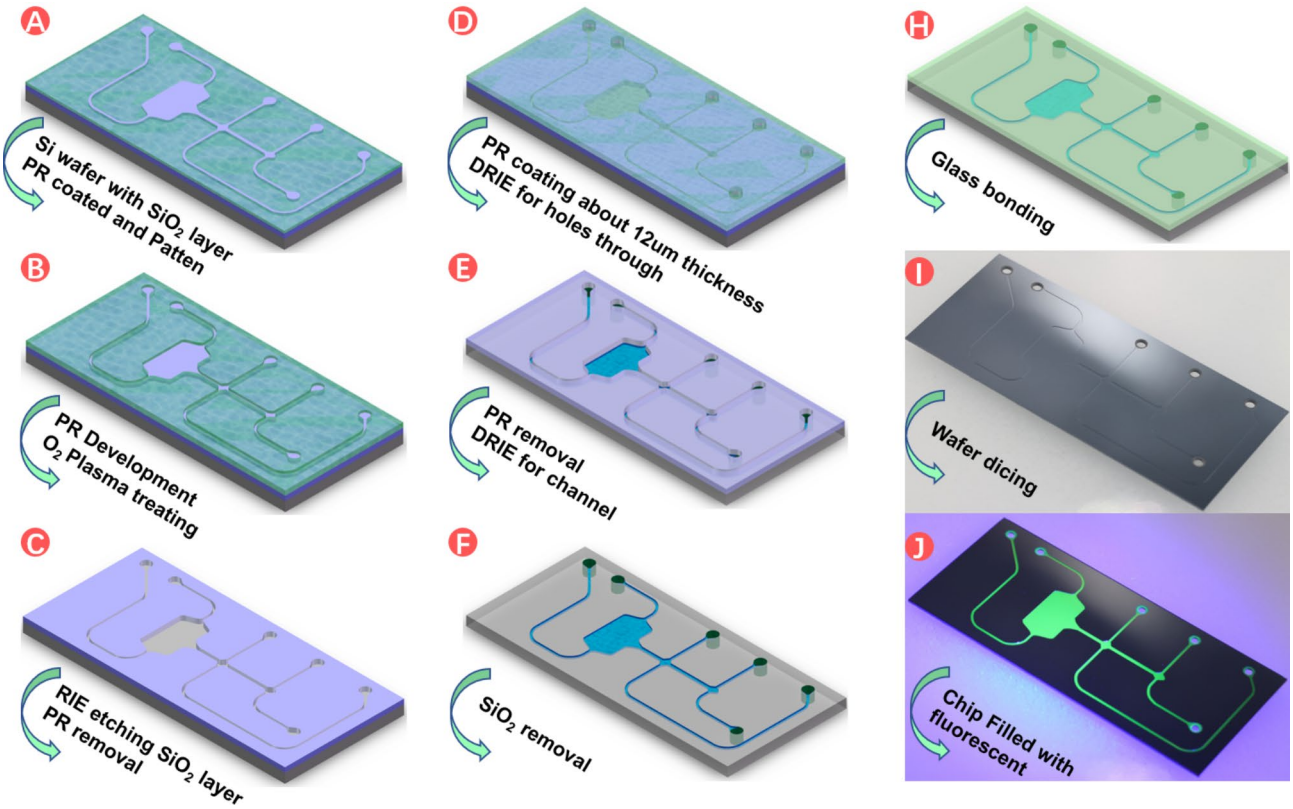

Fig. 5. Silicon-Glass Microfluidic Chip Fabrication Sequence: (**A**) Starting with a silicon wafer coated with SiO_2, the process involves photolithography, where we patterned a photoresist (PR) onto the SiO_2 surface. (**B**) followed by the PR development, and O_2 plasma was used to remove the PR undercut. (**C**) Etching was used to create microfluidic channels on the SiO_2 layer, and PR was removed. (**D**) A thick PR layer was coated, and holes were patterned on the wafer for DRIE to create a fluidics inlet and outlet. (**E**) PR removal. (**F**) Microchannel etching. (**H**) After removing the excess SiO_2 layer, the wafer was cleaned with an H_2SO_4 solution; the Pyrex type of glass was aligned with the Si wafer for anodic bonding, resulting in the finished microfluidic chip with precise channel architecture. (**I**) Wafer dicing of the Si-glass bonding sandwich to individual chips. (**J**) Fluorescence dye-filled Si-glass chip.

Material	λ ($W \cdot m^{-1} \cdot K^{-1}$)	c ($J \cdot kg^{-1} \cdot K^{-1}$)
Glass (soda lime)[55]	1.46	0.87
Si < 100 > [56]	139.4	0.71
PMMA [57]	0.19	1.48
PDMS [58]	0.16	0.88
H_2O	0.61	4.186

Table 2. Material properties.

Results and discussion

Results

We fabricated four different layouts of microfluidic chips for a sample to answer RNA/DNA extraction followed by DNA (RNA) amplification by (RT)-PCR or RT-LAMP made of PMMA-PMMA[33], PDMS-glass, glass-glass, and Si-glass.

We filled the first chip with black ink (Fig. 6A), the second with red ink (Fig. 6B), the third with blue ink (Fig. 6C), and the fourth with fluorescein solution with a concentration of ≈ 10 µM (Fig. 6D) we used white light for illumination except for the fourth chip, which was illuminated with blue light from a light-emitting diode (LED) with a nominal wavelength of ≈ 465 nm to increase the image contrast. A conventional single-lens reflex camera was used to capture all images.

Before the chip bonding, we determined the chamber surface roughness test using an atomic force microscope (Table 3) for PMMA (Fig. 6E) glass (Fig. 6F), PDMS (Fig. 6G), and Si (Fig. 6H). After processing, all chambers' surfaces, fabricated from four materials, have a very low roughness below ≈ 8 nm RMS, which is ≈ 3× lower than the surface roughness of a mirror. The Si surface also exhibited the lowest surface roughness, with all parameters summarized in Table 3.

Additionally, we also made a cross-section of PMMA-made channels (Fig. 6I) and captured an SEM image showing the nearly perfectly flat walls without any plane inequalities or increased roughness (Fig. 6J). We also filled PMMA-made channels with black ink to observe the integrity of the channels, indicating that there are no obstructions in the channel (Fig. 6K).

The four chips differ in properties and fabrication complexity (Fig. 7). We took optical images of all four chip channels using an objective with 5× magnifications and details of the channel edges using an objective with 20× magnifications, both in differential scanning contrast imaging mode, to increase the contrast between the channel and the surroundings. The chips made by CNC from PMMA (Fig. 7A), xurography using double sticky tape (Fig. 7B), DRIE from Si using Si-glass technology (Fig. 7C), and PDMS by 3D printing methods used for mold making (Fig. 7D). As expected, the best edge was formed by DRIE in Si as the line is defined by UV lithography followed by dry etching of Si. The second best line had the CNC-produced PMMA chip, followed by the PDMS-made device, and the worst was the xurographically-made device. On the other hand, the xurographically-made device is by far the cheapest one shown here. The PDMS-made chip can be produced with much better quality using the soft lithography technique, but we used much cheaper 3D printing for this work.

We used a fluorescence-based method to monitor the temperature increase and decrease inside the fabricated chips. Previously, we used the more precise photobleaching-free method based on a polymerase chain reaction master mix with an intercalating dye such as SYBR Green I or Eva Green[53]. Here, we were only interested in relative temperature change; thus, the fluorescein solution was sufficient[54].

We filled all chips with ≈ 10 µM fluorescein solution and placed them on the thermoelectric element to heat and cool The TEC was controlled by a LabView script developed for earlier work[59]. The sample was illuminated with the LED powered by current pulses with an amplitude of 40 mA, with a duty cycle of 50% utilizing a frequency of 1,012.1 Hz. The excited fluorescence was captured by a photomultiplier tube with a control voltage set to have the PMT with minimal gain to 0.5 V. Its voltage output corresponding to the fluorescence was processed by a lock-in amplifier to minimize the ambient light influence, and an oscilloscope monitored its output.

We first slowly increased the temperature of the chips from ≈ 40 °C to ≈ 70 °C using a temperature increase rate of ≈ 0.5 $K \cdot s^{-1}$ to determine the fluorescein temperature sensitivity. Then, we performed temperature cycling between ≈ 40 °C to ≈ 70 °C, achieving a ramping rate of the heater of ≈ 10 $K \cdot s^{-1}$ and ≈ − 5.9 $K \cdot s^{-1}$ for heating and cooling, respectively (Fig. 8A). The F as a function of T suffered from the photobleaching effect; thus, we performed a baseline determination and removal using Matlab script. The typical temperature profile of an F value is shown in Fig. 8B.

Then, we calculated the thermal time constant as the fluorescence amplitude followed an exponential function of first order:

$$F = F_0 - F_1 \cdot e^{-\frac{t-t_0}{\tau}}, \tag{2}$$

where F_0 and F_1 are fluorescence amplitude constants, t_0 is time at the beginning, and the τ value determines the heat transfer rate. We extracted the τ values from five consecutive measurements and calculated the standard deviation (σ) (Table 4).

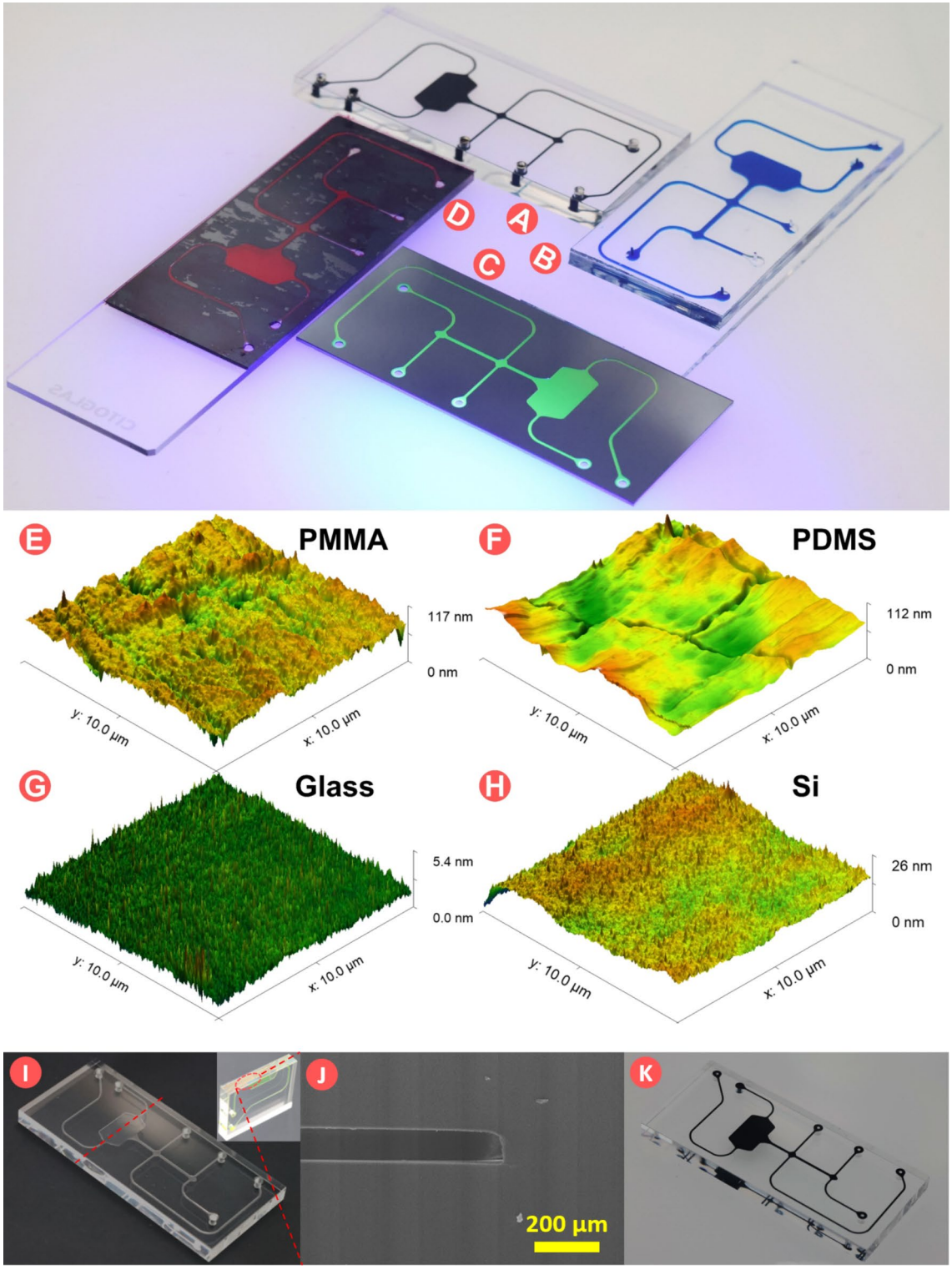

Fig. 6. Surface the roughness of all chips: (**A**) PMMA chips made by CNC machining and chemically assisted thermal bonding. (**B**) Double-sided tape cut by xurography forming channels between two glasses. (**C**) Si-glass-based microfluidics chip. (**D**) PDMS-glass chip by a 3D printer molding and O_2 plasma-assisted bonding. (**E**-**H**) 3D surface roughness of the PCR thermal chamber was measured using a Bruker atomic force microscope of PMMA chip, double side tape-glass chip, Si-glass chip, and PDMS-glass chip, respectively. (**I**) Cleaned PMMA hot-press bonded chip. (**J**) SEM cross-section image of the microfluidic chamber made in PMMA showing the high-quality bond between two PMMA layers as no original interface is visible. (K) The PMMA chip integrity test is done by filling the microfluidic channels and the chamber with black ink, and no visible leakage is observed.

Material	PMMA	Glass	PDMS	Si-glass
Roughness (nm)	7.19 ± 1.61	0.35 ± 0.07	4.44 ± 1.23	1.09 ± 0.20
Fabrication tolerance (µm).	5	20	25	0.5

Table 3. Surface roughness measurements of four different materials. Data were statistically analyzed from 10 spots with a size of (1 × 1) µm² without obvious impurities, cracks, or other damages.

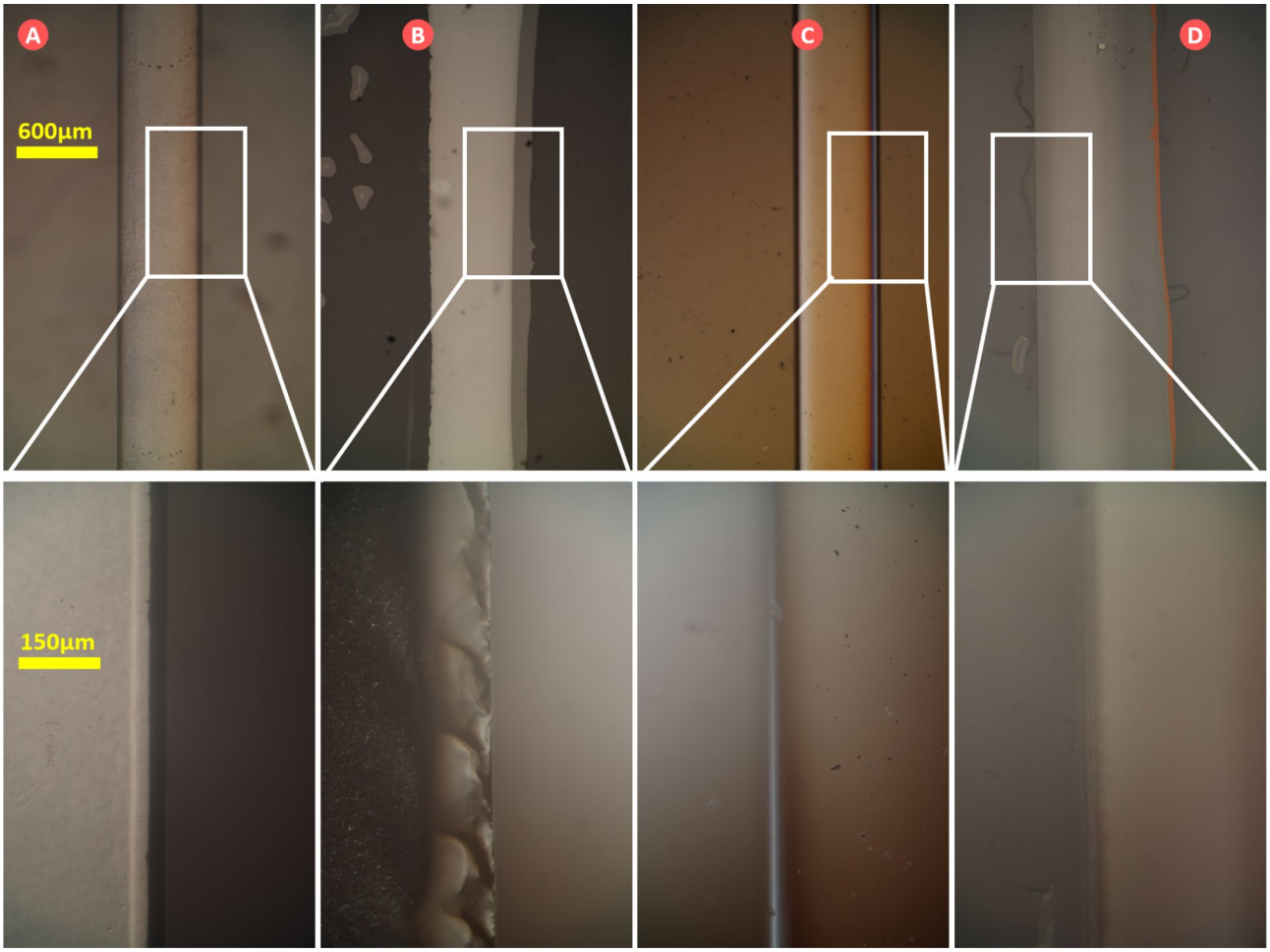

Fig. 7. Optical images of fabricated microfluidic channels. (Top) Images of the channels taken with a microscope objective lens with a magnification of 5× using differential interference contrast imaging mode (DIC); (Bottom) images of the channel edges taken with a microscope objective lens with a magnification of 20× in DIC mode: (**A**) a PMMA chip made by CNC machining and chemically assisted thermal bonding. (**B**) Xurographically made glass-to-glass interface formed by a double sticky tape. (**C**) Si-glass chip made by DRIE in Si. (**D**) PDMS chip using a mold made by 3D printing.

The fastest system is Si-glass, which was expected, and the slowest one is glass-glass, probably due to excessive glass thickness of 2 mm used for this study. An unusual temperature profile was found while using the PMMA-PMMA chip. While the heating thermal transfer seems normal, the cooling profile is strange as the fast cooling is followed by a different slope, probably caused by the PMMA – PMMA interface quality between individual layers related to the bonding method.

We recalculated the F value into T using a method previously employed based on two-point calibration[54]. We extracted the F_{0_MIN} and F_{0_MAX} values for heating and cooling to correlate them with the known minimum and maximum temperatures of the chip, which were 40.5 °C and 69.3 °C, respectively. We applied this linear function to recalculate the F into the T value (Fig. 8C).

Discussion

PDMS emerges as a favorable material for microfluidic chip fabrication, particularly due to its optical transparency, vital for microscopic analysis and optical sensing, and its minimal autofluorescence compared to

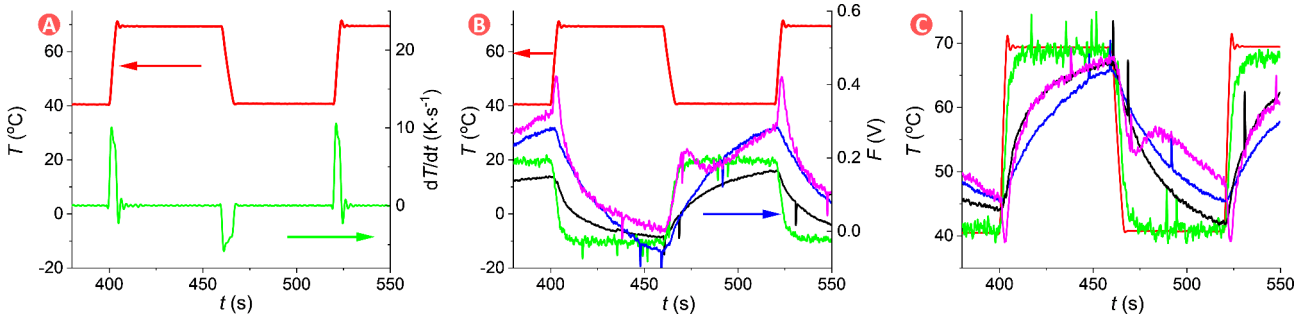

Fig. 8. Heating and cooling profiles of the TEC and the chips: (**A**) Heating and cooling of the TEC (red) and the heat ramping rate (green). (**B**) Monitoring F value at the PMT output in Si-glass (green), glass-glass (blue), PDMS-glass (black), and PMMA-PMMA (purple) chips used to calculate the thermal time constant. (**C**) The temperature of the TEC (red) and temperatures inside the Si-glass (green), glass-glass (blue), PDMS-glass (black), and PMMA-PMMA (purple) were calculated using the point method from the F amplitude of the fluorescein.

Material	Si-glass	Glass-glass	PDMS-glass	PMMA-PMMA
(τ ± σ) (s)	3.03 ± 0.48	39.32 ± 6.83	12.33 ± 0.47	15.86 ± 1.85

Table 4. Time constant values extracted from fluorescence as a function of temperature measurement.

PMMA[60]. However, its gas permeability, while advantageous for cell culture applications requiring gas exchange, poses challenges for applications needing a gas-impermeable environment. Despite its relatively straightforward fabrication process, which leads to lower material and production costs beneficial for prototyping or small-scale production, PDMS's absorption of hydrophobic molecules can interfere with specific analytical applications. Additionally, the production of PDMS chips still requires cleanroom facilities for mask-making and photoresist processing.

PMMA, known for its impressive optical transparency, enhances visual inspections and optical detection. However, its poor chemical resistance to common solvents[38] limits its use to water-based applications unless the channels are coated with parylene to improve chemical resistance and reduce molecule absorption[61], a technique also applied to PDMS. PMMA chips are produced using CNC milling, hot embossing, and injection molding, each catering to different production scales and requirements. CNC milling allows for complex designs without cleanroom facilities, making it ideal for prototyping and small production runs, though it involves higher initial setup costs. Hot embossing, suited for medium to high-volume production, requires a significant upfront investment in mold creation but offers excellent detail replication. Injection molding is optimal for high-volume production, providing cost efficiency at scale despite high initial mold costs. The choice of fabrication method for PMMA chips depends on the specific application requirements, production volume, and budget constraints.

Xurography, utilizing inexpensive materials like double-sided tape, offers a cost-effective solution for rapid prototyping without cleanroom requirements but lacks durability and design complexity. It is less suitable for mass production due to these limitations.

Silicon-glass chips, ideal for applications requiring high temperature and pressure resistance and excellent optical properties, involve a complex, multi-step fabrication process that requires specialized equipment like DRIE and cleanrooms. This makes them less favorable for rapid prototyping or budget-constrained projects due to their high cost and lengthy production times.

In summary, selecting a microfluidic chip fabrication method should consider the intended application, required scalability, material and fabrication costs, and turnaround times. For instance, PDMS is cost-effective for small-scale production, costing ≈ $1 - $5 per chip, and turnaround times from a few hours to a day, depending on complexity. PMMA, while offering scalability, varies in cost from $10 to $100 per mold for prototyping and much lower per-unit costs at higher volumes. CNC milling and hot embossing have longer setup times but provide more durable chips. Xurography is the least expensive and fastest for prototyping but offers limited functionality. Si-glass, while expensive—often exceeding $100 per chip for small batches—offers the best performance for demanding conditions.

Each material and method has strengths and is best suited to specific applications, necessitating a careful evaluation based on detailed cost analysis and functional requirements. For example, for high-precision diagnostic applications requiring chemical resistance and durability under thermal cycling, Si-glass is recommended, whereas, for educational models and proof-of-concept designs where cost and speed are crucial, xurography or CNC milling of PMMA may be more appropriate.

Conclusion

This comparative study of microfluidic chip fabrication techniques has introduced and summarized various methodologies tailored to specific applications. CNC machining provides a versatile approach for fabricating

PMMA devices, balancing detail-oriented design with scalability. Although PMMA and PDMS are recognized for their cost-efficiency and rapid production, it is essential to consider their material limitations against the demands of the intended application.

Silicon-glass microfluidics, notable for the highest levels of durability and performance, require significant investments in both time and capital, which may limit their accessibility for rapid prototyping. The selection of a fabrication technique must be driven by considerations of material properties, precision, cost, and device functionality to ensure an optimal solution is achieved.

As the demand for rapid, reliable, and accessible diagnostics grows, particularly in response to global health challenges like the COVID-19 pandemic, the value of adaptable microfluidic systems becomes increasingly evident. This work contributes significantly to the field by highlighting the capabilities and limitations of various fabrication techniques, thereby guiding the development of next-generation microfluidic devices that can meet the urgent and evolving needs of healthcare and research.

Our manuscript, while specialized, is intended for a broad audience encompassing a wide array of scientific disciplines beyond the niche fields. We aim to provide valuable insights into microfluidic chip fabrication and expand the research scope of scientists across various fields by comparing four different methods of fabricating microfluidic devices.

In conclusion, our research involved fabricating a variety of microfluidic devices using different materials and techniques—from straightforward CNC, which can be further simplified by hot embossing or injection molding, to more complex methods like xurography requiring glass drilling, and to time-intensive and costly soft lithography for PDMS molding and Si-glass technology. Each device exhibits unique properties due to the diverse materials utilized, showcasing the depth of our investigative approach.

Data availability

Data will be available upon a request from Pavel Neuzil: pavel.neuzil@gmail.com.

Received: 9 September 2024; Accepted: 18 November 2024
Published online: 20 November 2024

References

1. Whitesides, G. M. The origins and the future of microfluidics. *nature* 442, 368–373 (2006).
2. Sackmann, E. K., Fulton, A. L. & Beebe, D. J. The present and future role of microfluidics in biomedical research. *Nature* **507**, 181–189 (2014).
3. Zhang, H. et al. Nanolithography toolbox—Simplifying the design complexity of microfluidic chips. *J. Vacuum Sci. Technol. B Nanatechnol. Microelectronics: Mater. Process. Meas. Phenom.* **38**, 063002 (2020).
4. Scott, S. M. & Ali, Z. Fabrication methods for microfluidic devices: An overview. *Micromachines* **12**, 319 (2021).
5. Velten, T. et al. Roll-to-roll hot embossing of microstructures. *Microsyst. Technol.* **17**, 619–627 (2011).
6. Weisgrab, G., Ovsianikov, A. & Costa, P. F. Functional 3D printing for microfluidic chips. *Adv. Mater. Technol.* **4**, 1900275 (2019).
7. Suriano, R. et al. Femtosecond laser ablation of polymeric substrates for the fabrication of microfluidic channels. *Appl. Surf. Sci.* **257**, 6243–6250 (2011).
8. Thomas, L. E. et al. A glucose meter accuracy and precision comparison: The freestyle flash versus the accu-chek advantage, accu-chek compact plus, ascensia contour, and the BD logic. *Diabetes. Technol. Ther.* **10**, 102–110 (2008).
9. Ryan, F., O'SHEA, S. & Byrne, S. The reliability of point-of-care prothrombin time testing. A comparison of CoaguChek S® and XS® INR measurements with hospital laboratory monitoring. *Int. J. Lab. Hematol.***32**, e26–e33 (2010).
10. Carrilho, E., Martinez, A. W. & Whitesides, G. M. Understanding wax printing: A simple micropatterning process for paper-based microfluidics. *Anal. Chem.* **81**, 7091–7095 (2009).
11. Madhankumar, P., Sujatha, L., Sundar, R. & Viswanadam, G. Fabrication of low-cost MEMS microfluidic devices using metal embossing technique on glass for lab-on-chip applications. *J. Micromech. Microeng.* **33**, 084001 (2023).
12. Metz, S., Holzer, R. & Renaud, P. Polyimide-based microfluidic devices. *Lab. Chip*. **1**, 29–34 (2001).
13. Fan, Y., Li, H., Yi, Y. & Foulds, I. G. PMMA to polystyrene bonding for polymer based microfluidic systems. *Microsyst. Technol.* **20**, 59–64 (2014).
14. Lebedev, D. et al. Focused ion beam milling based formation of nanochannels in silicon-glass microfluidic chips for the study of ion transport. *Microfluid. Nanofluid.* **25**, 51 (2021).
15. Fornell, A., Söderbäck, P., Liu, Z., De Albuquerque Moreira, M. & Tenje, M. Fabrication of silicon microfluidic chips for acoustic particle focusing using direct laser writing. *Micromachines* **11**, 113 (2020).
16. Borók, A., Laboda, K. & Bonyár, A. PDMS bonding technologies for microfluidic applications: A review. *Biosensors* **11**, 292 (2021).
17. Nge, P. N., Rogers, C. I. & Woolley, A. T. advances in microfluidic materials, functions, integration, and applications. *Chem. Rev.* **113**, 2550–2583 (2013).
18. Kurita, R. & Niwa, O. Microfluidic platforms for DNA methylation analysis. *Lab. Chip*. **16**, 3631–3644 (2016).
19. Zhuang, J., Yin, J., Lv, S., Wang, B. & Mu, Y. Advanced lab-on-a-chip to detect viruses–current challenges and future perspectives. *Biosens. Bioelectron.* **163**, 112291 (2020).
20. Zeng, W., Jacobi, I., Beck, D. J., Li, S. & Stone, H. A. Characterization of syringe-pump-driven induced pressure fluctuations in elastic microchannels. *Lab. Chip*. **15**, 1110–1115 (2015).
21. Peng, R. & Li, D. Electrokinetic motion of single nanoparticles in single PDMS nanochannels. *Microfluid. Nanofluid.* **21**, 1–10 (2017).
22. Isiksacan, Z., Guler, M. T., Aydogdu, B., Bilican, I. & Elbuken, C. Rapid fabrication of microfluidic PDMS devices from reusable PDMS molds using laser ablation. *J. Micromech. Microeng.* **26**, 035008 (2016).
23. Chu, M., Nguyen, T., Lee, E., Morival, J. & Khine, M. Plasma free reversible and irreversible microfluidic bonding. *Lab. Chip*. **17**, 267–273 (2017).
24. Songjaroen, T., Dungchai, W., Chailapakul, O., Henry, C. S. & Laiwattanapaisal, W. Blood separation on microfluidic paper-based analytical devices. *Lab. Chip*. **12**, 3392–3398 (2012).
25. Ramdzan, A. N., Almeida, M. I. G., McCullough, M. J. & Kolev, S. D. Development of a microfluidic paper-based analytical device for the determination of salivary aldehydes. *Anal. Chim. Acta*. **919**, 47–54 (2016).
26. Yamada, K., Shibata, H., Suzuki, K. & Citterio, D. Toward practical application of paper-based microfluidics for medical diagnostics: State-of-the-art and challenges. *Lab. Chip*. **17**, 1206–1249 (2017).
27. Torul, H. et al. Paper membrane-based SERS platform for the determination of glucose in blood samples. *Anal. Bioanal. Chem.* **407**, 8243–8251 (2015).

28. Lin, Y. et al. Detection of heavy metal by paper-based microfluidics. *Biosens. Bioelectron.* **83**, 256–266 (2016).
29. Neuville, A. et al. Xurography for microfluidics on a reactive solid. *Lab. Chip*. **17**, 293–303 (2017).
30. Lei, K. F., Chang, C. H. & Chen, M. J. Paper/PMMA hybrid 3D cell culture microfluidic platform for the study of cellular crosstalk. *ACS Appl. Mater. Interfaces*. **9**, 13092–13101 (2017).
31. Fan, Y., Liu, Y., Li, H. & Foulds, I. G. Printed wax masks for 254 nm deep-UV pattering of PMMA-based microfluidics. *J. Micromech. Microeng.* **22**, 027001 (2012).
32. Nayak, N. C., Yue, C., Lam, Y. & Tan, Y. Thermal bonding of PMMA: Effect of polymer molecular weight. *Microsyst. Technol.* **16**, 487–491 (2010).
33. Sun, A. et al. An integrated microfluidic platform for nucleic acid testing. *Microsystems Nanoengineering*. **10**, 66 (2024).
34. Liu, X. et al. Smartphone integrated handheld (SPEED) digital polymerase chain reaction device. *Biosens. Bioelectron.* **232**, 115319 (2023).
35. Zhang, H. et al. SPEED: An integrated, smartphone-operated, handheld digital PCR device for point-of-care testing. *Microsystems Nanoengineering*. **10**, 62 (2024).
36. Girdwood, S. et al. The integration of tuberculosis and HIV testing on GeneXpert can substantially improve access and same-day diagnosis and benefit tuberculosis programmes: A diagnostic network optimization analysis in Zambia. *PLOS Global Public. Health*. **3**, e0001179 (2023).
37. Li, J. et al. Point-of-care testing of SARS-CoV-2 variants identified by XNA-Based RT-qPCR. *Archives Microbiol. Immunol.* **7**, 487–497 (2023).
38. Zhang, W. et al. PMMA/PDMS valves and pumps for disposable microfluidics. *Lab. Chip*. **9**, 3088–3094 (2009).
39. Fan, Y. Low-cost microfluidics: Materials and methods. *Micro Nano Lett.* **13**, 1367–1372 (2018).
40. TESA. *tesa® 61395*, https://www.tesa.com/en/industry/tesa-61395.html
41. Chen, C. S., Chen, S. C., Liao, W. H., Chien, R. D. & Lin, S. H. Micro injection molding of a micro-fluidic platform. *Int. Commun. Heat Mass Transfer*. **37**, 1290–1294 (2010).
42. Li, J. et al. Hot embossing/bonding of a poly (ethylene terephthalate)(PET) microfluidic chip. *J. Micromech. Microeng.* **18**, 015008 (2007).
43. Xia, Y. & Whitesides, G. M. Soft lithography. *Angew. Chem. Int. Ed.* **37**, 550–575 (1998).
44. Iliescu, C., Poenar, D. P., Carp, M. & Loe, F. C. A microfluidic device for impedance spectroscopy analysis of biological samples. *Sens. Actuators B*. **123**, 168–176 (2007).
45. Liu, X., Zhu, H., Sabó, J., Lánský, Z. & Neužil, P. Improvement of the signal to noise ratio for fluorescent imaging in microfluidic chips. *Sci. Rep.* **12**, 18911 (2022).
46. Gao, D., Liu, H., Jiang, Y. & Lin, J. M. Recent advances in microfluidics combined with mass spectrometry: Technologies and applications. *Lab. Chip*. **13**, 3309–3322 (2013).
47. Hu, X. et al. Fabrication of polyimide microfluidic devices by laser ablation based additive manufacturing. *Microsyst. Technol.* **26**, 1573–1583 (2020).
48. Riester, O., Laufer, S. & Deigner, H. P. Direct 3D printed biocompatible microfluidics: Assessment of human mesenchymal stem cell differentiation and cytotoxic drug screening in a dynamic culture system. *J. Nanobiotechnol.* **20**, 540 (2022).
49. Balram, K. C. et al. The nanolithography toolbox. *J. Res. Natl. Inst. Stand. Technol.* **121**, 464 (2016).
50. Al-Adhami, M., Andar, A., Tan, E., Rao, G. & Kostov, Y. A solvent-based method to fabricate PMMA microfluidic devices. *Lab. Chip* (2017).
51. Swaggard, T. et al. The name is bond – heat bond: Using a heated lamination press for thermoplastic thin film bonding. *Lab Chip* (2022).
52. Zhu, H. et al. Heat transfer time determination based on DNA melting curve analysis. *Microfluid. Nanofluid.* **24**, 1–8 (2020).
53. Neuzil, P., Cheng, F., Soon, J. B. W., Qian, L. L. & Reboud, J. Non-contact fluorescent bleaching-independent method for temperature measurement in microfluidic systems based on DNA melting curves. *Lab. chip*. **10**, 2818–2821 (2010).
54. Neužil, P., Sun, W., Karásek, T. & Manz, A. Nanoliter-sized overheated reactor. *Appl. Phys. Lett.* **106** (2015).
55. Prasad, A. et al. Thermal conductivity measurement of Soda–Lime–silica glass by transient 3 ω method with au Thin Film-based Micro-heater/Temperature Sensor fabricated by an innovative Approach. *Int. J. Thermophys.* **41**, 100 (2020).
56. Yamasue, E., Susa, M., Fukuyama, H. & Nagata, K. Thermal conductivities of silicon and germanium in solid and liquid states measured by non-stationary hot wire method with silica coated probe. *J. Cryst. Growth*. **234**, 121–131 (2002).
57. Assael, M., Botsios, S., Gialou, K. & Metaxa, I. Thermal conductivity of polymethyl methacrylate (PMMA) and borosilicate crown glass BK7. *Int. J. Thermophys.* **26**, 1595–1605 (2005).
58. Wei, J. et al. Enhanced thermal conductivity of polydimethylsiloxane composites with carbon fiber. *Compos. Commun.* **17**, 141–146 (2020).
59. Zhang, H. et al. Revealing the secrets of PCR. *Sens. Actuators B*. **298**, 126924 (2019).
60. Piruska, A. et al. The autofluorescence of plastic materials and chips measured under laser irradiation. *Lab. Chip*. **5**, 1348–1354 (2005).
61. Sasaki, H., Onoe, H., Osaki, T., Kawano, R. & Takeuchi, S. Parylene-coating in PDMS microfluidic channels prevents the absorption of fluorescent dyes. *Sens. Actuators B*. **150**, 478–482 (2010).

Acknowledgements

Pavel Neuzil would like to acknowledge the financial support from grant no. 52150710541 provided by the National Natural Science Foundation of PR China. Petra Vopařilová and other members of Mendel University would like to acknowledge financial support from the Internal Grant Agency of the Faculty of AgriSciences, Mendel University in Brno (No. AF-IGA2023-IP-030). The authors also thank for support from projects, National Centre for Biotechnology in Veterinary Medicine – NaCeBiVet (No. TN02000017) and the ERDF "Multidisciplinary research to increase application potential of nanomaterials in agricultural practice" No. CZ.02.1.0 1/0.0/0.0/16_025/0007314. Wen Zeng would like to acknowledge financial support from the Natural Science Foundation of Shaanxi Province (2023-JC-YB-306).

Author contributions

X.L. and A.S. did most experiments, J.B. and I.G. guided experiment, took care of graphics and came with the conclusion, T.L. made the PDMS chips, P.V. ran the biochemical experiments, O.Z> and Z.W. prepared together with P.N. the manuscipt. All co-authors reviewed the manuscript.

Declarations

Competing interests
The authors declare no competing interests.

Additional information
Correspondence and requests for materials should be addressed to I.G., W.Z. or P.N.

Reprints and permissions information is available at www.nature.com/reprints.

Publisher's note Springer Nature remains neutral with regard to jurisdictional claims in published maps and institutional affiliations.